Accurate measurement of pancreatic islet β-cell mass using a second-generation fluorescent exendin-4 analog

Thomas Reiner[a], Greg Thurber[a], Jason Gaglia[b,1], Claudio Vinegoni[a], Chong Wee Liew[c], Rabi Upadhyay[a], Rainer H. Kohler[a], Li Li[b], Rohit N. Kulkarni[c], Christophe Benoist[b], Diane Mathis[b,2], and Ralph Weissleder[a,d,2]

[a]Center for Systems Biology, Massachusetts General Hospital, Boston, MA 02114; and Departments of [b]Pathology and [d]Systems Biology, and [c]Joslin Diabetes Center, Harvard Medical School, Boston, MA 02115

Contributed by Diane Mathis, June 22, 2011 (sent for review May 26, 2011)

The hallmark of type 1 diabetes is autoimmune destruction of the insulin-producing β-cells of the pancreatic islets. Autoimmune diabetes has been difficult to study or treat because it is not usually diagnosed until substantial β-cell loss has already occurred. Imaging agents that permit noninvasive visualization of changes in β-cell mass remain a high-priority goal. We report on the development and testing of a near-infrared fluorescent β-cell imaging agent. Based on the amino acid sequence of exendin-4, we created a neopeptide via introduction of an unnatural amino acid at the K_{12} position, which could subsequently be conjugated to fluorophores via bioorthogonal copper-catalyzed click-chemistry. Cell assays confirmed that the resulting fluorescent probe ($E4_{\times 12}$-VT750) had a high binding affinity (~3 nM). Its in vivo properties were evaluated using high-resolution intravital imaging, histology, whole-pancreas visualization, and endoscopic imaging. According to intravital microscopy, the probe rapidly bound to β-cells and, as demonstrated by confocal microscopy, it was internalized. Histology of the whole pancreas showed a close correspondence between fluorescence and insulin staining, and there was an excellent correlation between imaging signals and β-cell mass in mice treated with streptozotocin, a β-cell toxin. Individual islets could also be visualized by endoscopic imaging. In short, $E4_{\times 12}$-VT750 showed strong and selective binding to glucose-like peptide-1 receptors and permitted accurate measurement of β-cell mass in both diabetic and nondiabetic mice. This near-infrared imaging probe, as well as future radioisotope-labeled versions of it, should prove to be important tools for monitoring diabetes, progression, and treatment in both experimental and clinical contexts.

peptide | targeted imaging probe | near-infrared fluorophore | islets of Langerhans | GLP-1 receptor

Type 1 (or autoimmune) diabetes is characterized by T lymphocyte-dependent β-cell loss, leading to insulin deficiency. Despite its prevalence, however, many questions regarding the etiology and pathogenesis of this disorder remain unanswered. Disease triggers have not yet been identified, and there is only a limited understanding of the genetic and environmental factors that influence progression. Furthermore, because only indirect methods are currently available for monitoring the influence of therapeutical interventions, clinical trials tend to be long and expensive. For these reasons, the noninvasive imaging and quantification of β-cell mass in vivo has been considered a high priority in this field of investigation.

There continues to be a lack of universal and clinically translatable imaging agents and approaches for reliably visualizing β-cells. Previously developed β-cell–specific imaging agents have included labeled glucose analogs (or other small molecules) (1, 2), antibodies (3), sulfonylureas (2, 4), and vesicular monoamine transporter receptor agonists (5, 6). In addition, a variety of transgenic strategies have been applied to mouse models (7, 8). Some of these compounds have already been tested clinically with PET imaging (1, 9, 10). However, a prevailing problem with most injectable agents has been the inability of whole-body imaging studies to achieve a target-to-background ratio sufficiently high to detect the <2% of the pancreatic volume composed of β-cells (2). Recent developments in this area have been summarized in several reviews (11–13).

The following technologies have also been advocated because they provide higher spatial resolutions: intravital microscopy (14, 15); tomographic fluorescence imaging at the whole-body (16) or isolated-organ level (17, 18); and, more recently, fiberoptic imaging (19). Several fluorescent imaging agents that rely on such technologies have been described (20, 21). Based on the clinical success seen with glucagon-like peptide 1 (GLP-1) agonistic approaches (22), we previously designed both dipeptidyl peptidase-4 (23) and GLP-1 receptor (GLP-1R) imaging agents (24). GLP-1R is a receptor that is highly expressed on the surface of pancreatic β-cells, and one that binds to the peptide exendin-4 with nanomolar affinity (22, 25). GLP-1R has also become an important druggable target for the treatment of type 2 diabetes (exenatide, Byetta; Amylin/Eli Lilly). Given the high density of these receptors on β-cells, GLP-1R has likewise emerged as a promising target for imaging. However, converting affinity ligands into imaging agents has thus far proven challenging because of difficulties in selective synthesis, analysis, and purification. In the present study, we report on the design and in vivo testing of a next-generation exendin neopeptide for optical imaging and quantification of β-cell mass.

Results

Synthesis and Analysis of $E4_{\times 12}$-VT750. The amino acid lysine at the 12 position (K_{12}) of the exendin-4 sequence can be used as a modification point without significant reduction of peptide/GLP-1R target binding (22, 24). Based on earlier findings, this is in contradistinction to fluorochrome modification of a lysine group at the 40 position (K_{40}), which has been shown to affect target selectivity (24), presumably because of the close proximity of this lysine group to the extracellular domain of the GLP-1R binding site. To facilitate site-specific K_{12} labeling, we designed a neopeptide, $E4_{\times 12}$, which allows attachment of desired markers via Copper(I)-catalyzed azide-alkyne cycloaddition reactions (CuAAC) (26). Based on the exendin-4 sequence, we replaced K_{12} with the unnatural alkyne-amino acid (*S*)-2-amino-4-pentynoic acid. Simple CuAAC conditions (aqueous buffer, $CuSO_4$, L-ascorbic acid) allowed attachment of the azide-functionalized near-infrared (NIR) fluorophore (VT750) to $E4_{\times 12}$. This pro-

Author contributions: T.R., G.T., J.G., C.V., C.W.L., R.U., R.H.K., L.L., R.N.K., C.B., D.M., and R.W. designed research; T.R., G.T., J.G., C.V., C.W.L., R.U., R.H.K., L.L., R.N.K., C.B., D.M., and R.W. performed research; T.R. and R.W. contributed new reagents/analytic tools; T.R., G.T., J.G., C.V., C.W.L., R.U., R.H.K., L.L., R.N.K., C.B., D.M., and R.W. analyzed data; and T.R., G.T., J.G., C.V., C.W.L., R.U., R.H.K., L.L., R.N.K., C.B., D.M., and R.W. wrote the paper.

The authors declare no conflict of interest.

[1]Present address: Joslin Diabetes Center, Harvard Medical School, Boston, MA 02215.

[2]To whom correspondence may be addressed. E-mail: dm@hms.harvard.edu or rweissleder@mgh.harvard.edu.

This article contains supporting information online at www.pnas.org/lookup/suppl/doi:10.1073/pnas.1109859108/-/DCSupplemental.

duced the NIR GLP-1R probe with an overall synthetic yield of 64% from starting materials. HPLC/electrospray ionization/MS and MALDI/MS confirmed the identity of $E4_{\times 12}$-VT750 and gave a mass-to-charge ratio corresponding to the calculated mass (synthetic details are provided in *SI Research Design and Methods*).

Binding, Affinity, and Inhibition. Cell assays were performed using the MIN6 cell line, which naturally expresses GLP-1R, HEK/human GLP (hGLP)-1R cells that ectopically express GLP-1R and GLP-1R–negative NIH 3T3 cells. Incubation of each line with different concentrations of $E4_{\times 12}$-VT750 revealed increasing fluorescence for MIN6 and HEK/hGLP-1R cells, whereas no increase in fluorescence was detectable for NIH 3T3 cells (Fig. 1*A*). The IC_{50} values for both MIN6 and HEK/hGLP-1R cells were 3.3 ± 1.3 nM. To probe the selectivity of $E4_{\times 12}$-VT750 for GLP-1R, we first incubated both MIN6 and HEK/hGLP-1R cells with different concentrations of exendin-4 (0 nM to 500 nM) and a fixed concentration of $E4_{\times 12}$-VT750 (10 nM; Fig. 1*B*). On preincubation with exendin-4, a concentration-dependent decrease in $E4_{\times 12}$-VT750 fluorescence signal was observed. Indeed, preincubation with 500 nM exendin-4 (a 50-fold excess of exendin-4 relative to $E4_{\times 12}$-VT750) produced a near-quantitative reduction in fluorescence signal. These results show not only that $E4_{\times 12}$-VT750 was selectively taken up by GLP-1R–expressing cell lines but that its uptake could be selectively inhibited on addition of the unlabeled analog. Binding of GLP-1 to GLP-1R resulted in internalization of the peptide into cells and its localization in endosomal compartments (26). To visualize the cellular localization of $E4_{\times 12}$-VT750, we incubated HEK/hGLP-1R (Fig. 1*C*) with a 10-nM solution of $E4_{\times 12}$-VT750 for 90 min. Cells were stained with CellTracker Green (Invitrogen) to visualize the cell boundaries. The fluorescent probe $E4_{\times 12}$-VT750, like GLP-1, could be identified inside β-cells in vesicular compartments (Fig. 1*C*, *Upper*). In contrast, similar to what was seen with competitive binding assays (Fig. 1*B*), preincubation with unlabeled exendin-4 suppressed the $E4_{\times 12}$-VT750 fluorescence signal (Fig. 1*C*, *Lower*).

Pharmacokinetics. Under in vivo conditions, $E4_{\times 12}$-VT750 accumulated rapidly and selectively in both islets and β-cells, as confirmed by colocalization with the mouse insulin 1 promoter (MIP)-GFP signal (Fig. 2 *A*–*D*). Pancreata of live MIP-GFP mice were then exteriorized, and intact blood flow was confirmed through an injection of Angiosense 680 (PerkinElmer). After focusing on an islet, mice were injected with $E4_{\times 12}$-VT750 (2–4 nmol per 200 μL) and islet signal intensity was measured over time. $E4_{\times 12}$-VT750 was seen to accumulate in pancreatic β-cells within 10 min, reaching a plateau at ∼15 min (Fig. 2*E*). At 2 h after injection, the islet signal had increased ∼64-fold over background. The blood concentration of $E4_{\times 12}$-VT750 followed a biexponential decay pattern, giving a weighted $t_{1/2}$ of 84.4 s (Fig. 2*F*).

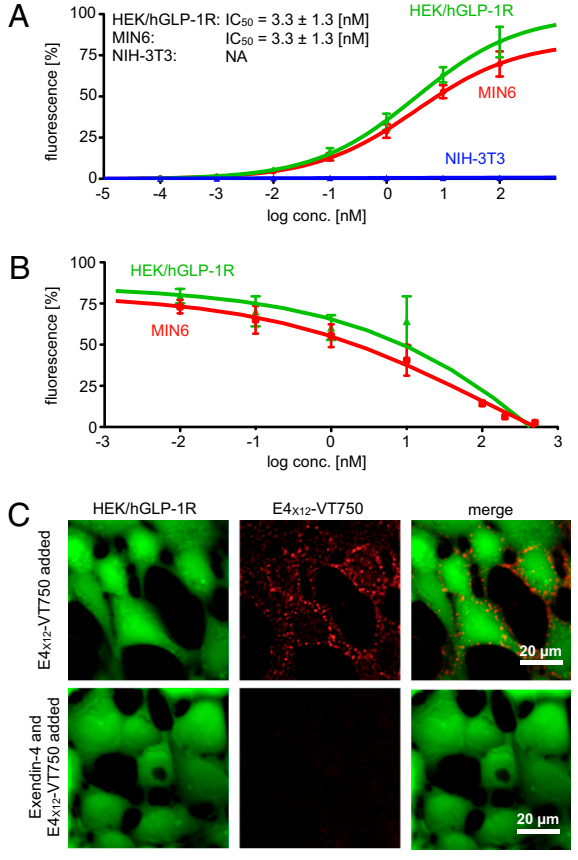

Fig. 1. Binding, affinity, and inhibition. (*A*) Cell-binding assays of different concentrations of $E4_{\times 12}$-VT750 against HEK/hGLP-1R (GLP-1R overexpressing), MIN6 (naturally expressing GLP-1R), and NIH 3T3 (GLP-1R–negative). (*B*) In vitro blocking experiments of $E4_{\times 12}$-VT750/GLP-1R binding ($E4_{\times 12}$-VT750 = 10 nM) with different concentrations of exendin-4. (*C*) Cell imaging experiments of HEK/hGLP-1R cells following incubation with $E4_{\times 12}$-VT750 (red) alone (*Upper*) or after preincubation with excess exendin-4 (*Lower*). Green, whole cell stain.

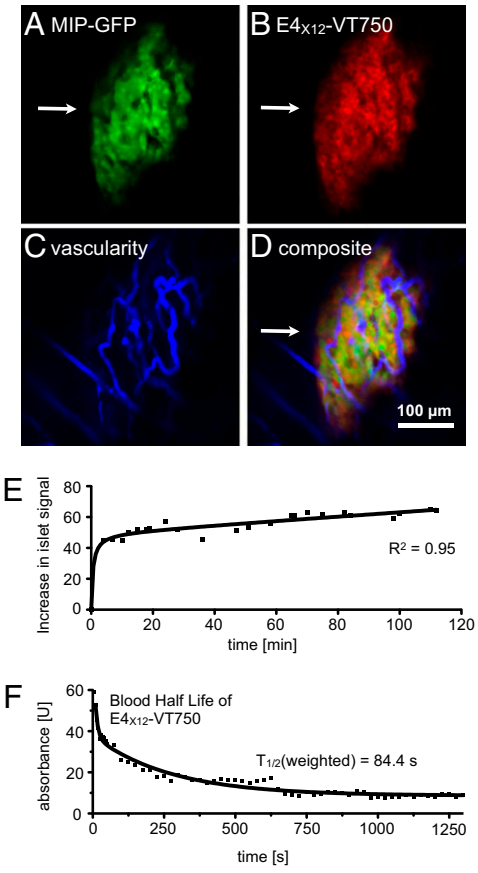

Fig. 2. Pharmacokinetics. (*A*–*D*) Intravital confocal imaging of a pancreatic islet (arrows) in a live MIP-GFP mouse. Green, GFP signal from MIP-GFP–positive pancreatic β-cells; red, $E4_{\times 12}$-VT750 (0.2 nmol/g); blue, fluorescent vascular agent. All images were acquired with an objective with a magnification of 20× in anesthetized live mice. (*E*) Increase in islet signal following a dose of systemic $E4_{\times 12}$-VT750 injection. (*F*) Blood half-life measurement of $E4_{\times 12}$-VT750 (0.2 nmol/g) injected into a MIP-GFP mouse.

The organ distribution of $E4_{\times 12}$-VT750 was estimated by measuring the 750-nm fluorescence in excised organs [mean fluorescence units × A^2] and comparing that 60 min after i.v. injection with the autofluorescence of noninjected normal mice. The comparative fluorescence distribution was as follows: kidney (69.0%), liver (14.8%), pancreas (7.9%), intestine (3.7%), lungs (2.6%), and stomach (1.7%). The NIR fluorophore uptake in both the spleen and heart was <1%. Serial imaging data suggested that the primary excretion pathway for $E4_{\times 12}$-VT750 was predominantly renal, based on the high quantities of probe in the bladder and kidney; this is consistent with the compound's size and blood half-life.

Validation. To correlate probe uptake in pancreatic β-cells quantitatively, we performed image analysis of MIP-GFP mice. Mice were sacrificed 40 min after i.v. injection of the probe, and their pancreata were removed and sectioned for imaging. Signal in the 488-nm channel (Fig. 3*A*) represented insulin promoter-driven GFP expression, an indicator of islet area, whereas signal in the 750-nm channel (Fig. 3*B*) read out probe uptake. Figs. 3 *C* and *D* show the H&E staining and anti-insulin staining of an adjacent histological slide, respectively. There was an excellent correlation between the islet sizes as determined by areas in the GFP and VT750 channels from GFP expression (R^2 = 0.992; Fig. 3*E*). We found a similar excellent correlation between $E4_{\times 12}$-VT750 signal intensities and islet areas estimated from GFP expression. (R^2 = 0.944; Fig. 3*F*). When mice were injected with unlabeled exendin-4 (15 nmol) before injection with $E4_{\times 12}$-VT750 (2 nmol), however, no uptake of imaging agent was observed in pancreatic β-cells. Therefore, this confirmed the selective binding of the fluorescent reporter to GLP-1 receptors in vivo.

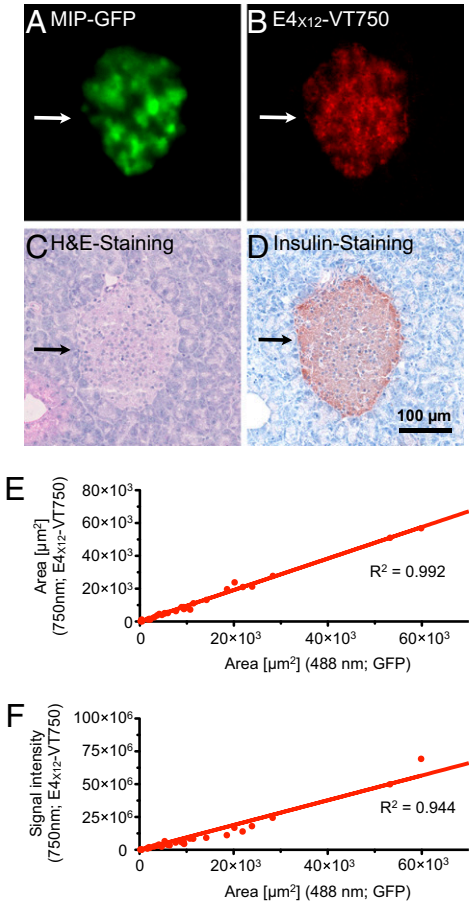

Fig. 3. GFP and probe colocalization in $E4_{\times 12}$-VT750–injected MIP-GFP mice. (*A* and *B*) Fluorescence, histology of harvested pancreas (green, MIP-GFP; red, $E4_{\times 12}$-VT750). The arrow points to H&E staining of a single islet (*C*) and antiinsulin staining of the same islet (*D*) using adjacent sections. (*E*) Correlation of islet sizes estimated via the MIP-GFP reporter (488 nm) vs. the GLP-1R probe $E4_{\times 12}$-VT750 (750 nm). (*F*) Correlation of islet sizes observed with the MIP-GFP reporter (488 nm) vs. signal intensity observed at 750 nm in the same area.

Loss of β-Cell Mass. To determine whether the probe could also be used to measure loss of β-cell mass, we compared $E4_{\times 12}$-VT750 accumulation (measured via whole-pancreas imaging) and β-cell mass (quantified by histology) with and without streptozotocin (STZ) administration to B6 mice. STZ rather specifically kills pancreatic islet β-cells, eventually resulting in insulin-dependent diabetes (27). Fig. 4 *A* and *B* shows representative examples of islets and surrounding exocrine pancreas tissue at two different resolutions, illustrating that $E4_{\times 12}$-VT750 stains pancreatic islets with high specificity. Fig. 4*C* summarizes image analysis from various cohorts of mice treated with different amounts of STZ. The NIR fluorescence decreased with increasingly aggressive STZ treatment. Mice were normoglycemic (blood-glucose levels <250 mg/dL) at the lowest STZ dose and hyperglycemic at the higher doses (Fig. 4*C*). Compared with immunohistochemical estimation of β-cell mass via antiinsulin staining (Fig. 4 *D* and *E*), there was a good correlation between observed fluorescence intensity for $E4_{\times 12}$-VT750 and β-cell mass (R^2 = 0.854, P < 0.0001; Fig. 4*E*). These data show that probe accumulation correlates with β-cell mass and is sensitive enough detect a β-cell mass loss in mice that are still normoglycemic (<25% loss of β-cell mass is detectable at a 99% confidence interval; Fig. 4*E*).

Fiberoptic Imaging. To test the feasibility of fiberoptic islet imaging and/or confocal microscopy endoscopic imaging, we tested the probe in live mice using a custom-built single-channel (680 nm) microendoscopic imaging system. MIP-GFP mice were injected with $E4_{\times 12}$-VT750 via a tail vein (0.2 nmol/g), and their pancreata were examined. The results showed that the NIR fluorescence signal could be clearly detected and was colocalized with the GFP signal using a separate confocal microscope but having two optical channels (Fig. 5; 480 and 680 nm). This system could thus potentially be used in endoscopic (i.e., imaging pancreatic parenchyma through duodenal sweep or via pancreatic duct), laparoscopic, or intraoperative settings to map surface located islets.

Discussion

Abundantly and selectively expressed cell-surface receptors have been shown to be good imaging targets, particularly when affinity ligand interaction triggers internalization of the imaging probe and when tissues are well perfused (28, 29). GLP-1R represents one such example, given its high expression, intrapancreatic specificity, and internalization (22). $E4_{\times 12}$-VT750 is a prototype second-generation GLP-1R–targeted imaging probe and is based on a K_{12}-modified neopeptide. We show that (*i*) this probe can be easily synthesized; (*ii*) fluorochrome labeling is site-specific; (*iii*) synthetic yields are high; and (*iv*) the probe is sufficiently bright and red-shifted for in vivo use, particularly in intravital microscopy and endoscopic imaging. In previous work, we developed first-generation fluorescent β-cell probes (24) for initial proof-of-principle studies. However, in comparison with the second-generation probes described here, the earlier ones had a number of significant drawbacks. For example, our previous probes used Byetta as the starting material, which, on hydroxysuccinimide ester modification, resulted in mixtures requiring laborious purification. In addition, our earlier probes contained a 680-nm fluorochrome, which was less well suited to in vivo imaging, not only because there is reduced tissue autofluorescence at a wavelength of 750 nm but because there is higher tissue penetration at 750–800 nm. Finally, the synthetic yields of the second-generation probes are 92% higher than those of previous compounds.

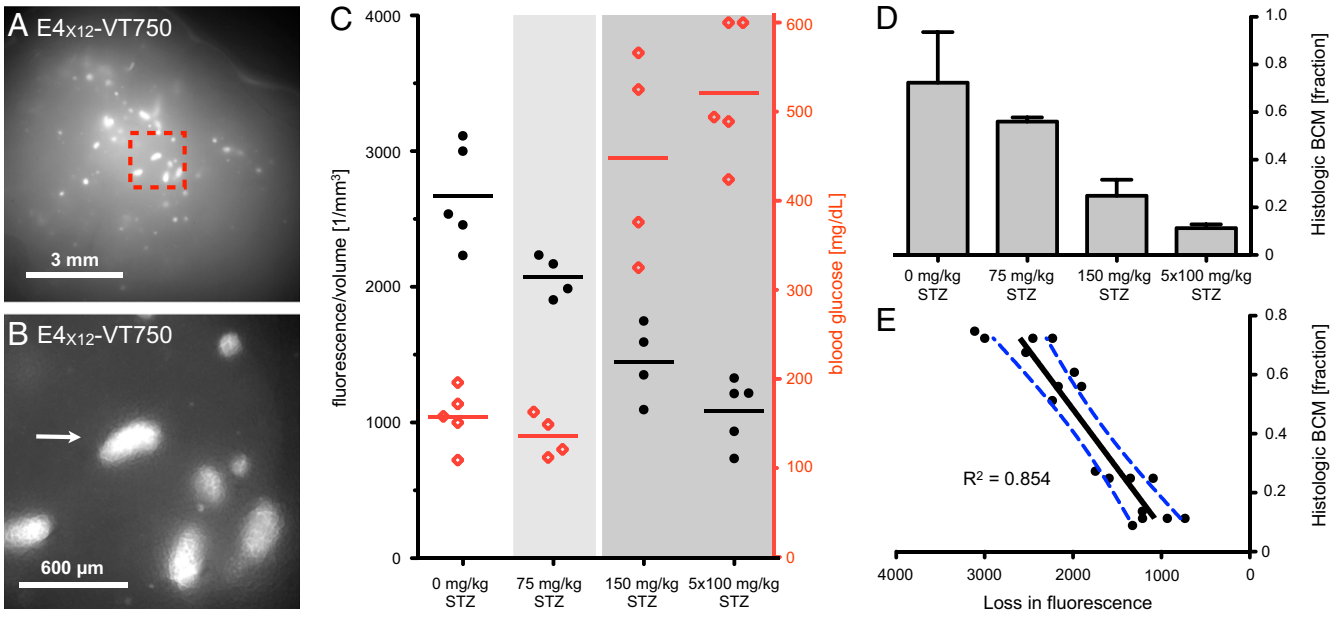

Fig. 4. $E4_{\times12}$-VT750 and histological β-cell mass quantification. (*A*) Typical staining patterns observed for pancreata injected with $E4_{\times12}$-VT750 (0.1 nmol/g, 40 min, mouse perfused and pancreas flushed) and imaged via surface reflectance microscopy. Note the very high target accumulation and very low background. (*B*) Higher magnification of a section from *A*, as indicated by the dashed box. The arrow points to a single islet. (*C*) Quantitative fluorescence signals (750 nm) were observed in pancreata of diabetic and nondiabetic mice injected with $E4_{\times12}$-VT750 (0.1 nmol/g, 40 min, mouse perfused and pancreas flushed; $P < 0.0001$) [light gray, STZ-treated but nondiabetic mice (blood glucose levels <200 mg/dL); darker gray, overt diabetic mice (blood glucose levels >300 mg/dL)]. Blood glucose levels are indicated by ♢ symbols ($P < 0.0001$). (*D*) β-Cell mass, as estimated from histology of untreated mice and mice treated with different concentrations of STZ. (*E*) Correlation of β-cell mass quantification data from immunohistochemical staining and from $E4_{\times12}$-VT750 fluorescence measurements (blue line, 99% confidence bands). BCM, β-cell mass.

Recent years have seen the successful introduction of therapies targeting the guanine nucleotide-binding protein (G protein)–coupled GLP-1 receptor within islet β-cells. Exendin-4, isolated from the Gila monster, shares ~53% sequence homology with mammalian GLP-1. It also binds to the GLP-1 receptor with the same affinity as native GLP-1. A synthetic form of exendin-4 (exenatide) was approved by the US Food and Drug Administration in 2005 for the treatment of type 2 diabetes.

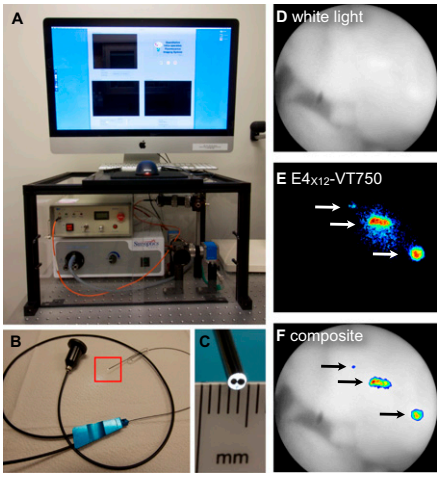

Fig. 5. Intravital pancreatic laparoscopy in a live MIP-GFP mouse. (*A*) Intravital imaging system. (*B*) Endoscopic imaging probe. (*C*) Higher magnification of the imaging probe head (outer diameter = 1.6 mm, probe head indicated in *B* by red box). (*D*) Field of view under white light conditions. (*E*) NIR fluorescence signal in islets (arrows) of the same area as in *D*. Note that the fiberoptic scope only has NIR channel fluorescence and white light capability. (*F*) Composite image. Arrows point to three distinct islets in this field of view.

Since then, a number of other exendin-4 analogs have been developed with the aim of prolonging the half-life of therapeutical action. Modifications have included aminoisobutyric acid modification of R_2 and R_{28} (Taspoglutide; Roche), R_4 modification with a C16 fatty acid (Liraglutide; Novo Nordisk), conjugation to albumin (CJC-1134; Albugon), and the use of nanomaterial-based release systems (exenatide LAR; Amylin/Eli Lilly). These studies, systematic amino acid substitutions, and crystallographic data have consequently enabled the more rational design of newer analogs possessing different biological properties. Based on these insights and on previous data indicating that the C-terminal end is needed for target specificity, we designed the $K_{12}\rightarrow X_{12}$ modification.

$E4_{\times12}$-VT750 has ideal pharmacokinetic and imaging characteristics. It exhibits high-affinity receptor–mediated cellular internalization and trapping, and it has a short half-life with minimal nonspecific tissue accumulation. In the present study, we showed that $E4_{\times12}$-VT750 can also be imaged within minutes to hours of i.v. administration. We thus anticipate that it can be adapted for a number of different applications. For example, $E4_{\times12}$-VT750 may be a useful reagent for the rapid intravital staining of islets, particularly in mouse models that do not express a fluorescent reporter. This application is particularly advantageous for the NOD mouse model of type 1 diabetes, where crossing in a fluorescent marker routinely entails on the order of 10 backcrosses. The compound also works well in frozen tissue sections. Likewise, we showed that achievable islet-to-background ratios were high enough for fiberoptic imaging; this property could have clinical utility. Both laparoscopic imaging and endomicroscopy are rapidly advancing techniques (30, 31) that will benefit greatly from target-specific fluorescent probes. We also envision that the probe may have utility for intraoperative fluorescence imaging of both islets and islet tumors (32, 33). Moreover, the probe may be uniquely applied to the imaging of pancreatic or islet transplants. Finally, it is possible that this probe (or related compounds) can be used for testing

the efficacy of novel therapeutics aimed at reversing insulitis and preserving β-cell mass. To this end, we are therefore also experimenting with isotope-labeled versions of the compound based on the second-generation scaffold presented here.

Research Design and Methods

Cell Culture. Mouse insulinoma-derived MIN6 cells (34) were used between passages 26 and 40 and were grown in high-glucose DMEM containing 15% (vol/vol) heat-inactivated FBS, 50 U/mL penicillin, and 10 μg/mL streptomycin. HEK cells stably expressing hGLP-1R (HEK/hGLP-1R) (35) were grown in high-glucose DMEM containing 10% (vol/vol) heat-inactivated FBS, 50 U/mL penicillin, 10 μg/mL streptomycin, 1 mM sodium pyruvate, and 150 μg/mL G418 (geneticin). GLP-1R–negative NIH 3T3 fibroblasts (ATCC) were grown in high-glucose DMEM containing 10% (vol/vol) heat-inactivated FBS, 50 U/mL penicillin, and 10 μg/mL streptomycin.

Cell-Labeling Assays. MIN6 (1×10^5 cells per well), HEK/hGLP-1R (3×10^4 cells per well), or NIH 3T3 (3×10^4 cells per well) cells were seeded into 96-well plates and incubated for 48 h before incubation with various concentrations of $E4_{\times 12}$-VT750 for 90 min at 37 °C. Following incubation, cells were washed once with PBS and the fluorescence levels were measured with a SynergyMx (Biotek) plate reader at an excitation of 755 nm and emission of 775 nm. After measurement of fluorescence, proteins were extracted using radioimmunoprecipitation assay lysis buffers (36), and protein levels were determined using a bicinchoninic acid assay (Thermo Fisher Scientific).

Blocking Experiments. MIN6 (1×10^5 cells per well) or HEK/hGLP-1R (3×10^4 cells per well) cells were seeded into 96-well plates and cultured for 48 h. The cells were then incubated with $E4_{\times 12}$-VT750 (10 nM) for 90 min at 37 °C alone or with increasing doses of exendin-4 (exenatide; 0 nM to 500 nM) for 1 h at 37 °C and subsequently with $E4_{\times 12}$-VT750 (10 nM) for 90 min at 37 °C. Following incubation, cells were imaged and proteins were quantified as described above.

Cell Imaging. MIN6 (2×10^5 cells per well), HEK/hGLP-1R (7.5×10^4 cells per well), or NIH 3T3 (7.5×10^4 cells per well) cells were seeded onto eight-well chamber slides (LabTek) and cultured for 48 h (at 37 °C). The cells were then incubated with 10 nM $E4_{\times 12}$-VT750 (90 min at 37 °C) alone or underwent an initial incubation with 3.5 μM exendin-4 (30 min at 37 °C and washed 1 time with growth medium) before subsequent incubation with 10 nM $E4_{\times 12}$-VT750 (90 min at 37 °C). The cells were then washed once with growth medium and once with 1× PBS. MIN6, HEK/hGLP-1R, and NIH 3T3 cells were imaged using an intravital laser scanning microscope (IV100; Olympus Corporation) (37).

Animals. Both C57BL/6J (B6) mice and B6.Cg-Tg(Ins1-EGFP)1Hara/J mice (38), which express EGFP within the islets under MIP-GFP, were obtained from the Jackson Laboratory. All procedures and animal protocols were approved by the subcommittee on Research Animal Care at Massachusetts General Hospital.

Animal Preparation. Mice were anesthetized with 2% isoflurane (vol/vol) and 2 L/min O_2. The peritoneal cavity was opened with a transverse incision in the disinfected abdominal wall. The gastric-splenic ligament was then dissected, and the pancreas was carefully exteriorized for intravital microscopy. Robust blood flow was observed in the pancreatic arteries for the duration of each experiment, and pancreas perfusion was confirmed by the presence of a circulating fluorescent vascular agent (Angiosense 680). The exteriorized pancreas was then completely submerged in temperature-controlled lactated Ringer's solution. The temperature near the spleen was carefully monitored using an Omega HH12A thermometer with fine wire thermocouples (Omega Engineering, Inc.) and maintained at 37 °C. A tail vein catheter, made using a 30-gauge × 1/2-inch needle inserted into BD intramedic Polyethylene10 tubing, was inserted before surgery. Via this tail vein catheter, 200 μL (2–4 nmol per 200 μL) of $E4_{\times 12}$-VT750 was subsequently injected either with or without preinjection of exendin-4 (15 nmol per 200 μL).

Intravital Laser-Scanning Microscopy. Images were collected with an intravital laser-scanning microscope (IV100) (37) using an Olympus UPlanFL (0.5 N.A.) objective with a magnification of 20×. Samples were excited at 488 nm with an air-cooled argon laser (Melles Griot) for visualization of either GFP-expressing islet cells or cells stained with Celltracker Green CMFDA (Invitrogen). The samples were also excited at 748 nm with a red diode laser (model FV10-LD748; Olympus Corporation) for visualization of $E4_{\times 12}$-VT750. Light was collected using custom-built dichroic mirrors SDM-560 and SDM-750 and emission filters BA 505–550 and BA 770 nm IF (Olympus Corporation). The green and red signals were collected sequentially to avoid bleed-through into the VT750 channel. A prototypical tissue stabilizer (Olympus Corporation) was used to reduce motion artifacts and to stabilize the focal plane. The stabilizer was attached to the objective, and its z-position was finely adjusted using a micrometer screw to apply soft pressure on the tissue.

Image Analysis. The accumulation of the $E4_{\times 12}$-VT750 probe within islets was determined by intravital imaging in MIP-GFP mice, as described above, using an Olympus UPlanFl (0.3 N.A.) objective at a magnification of 10×. Images before probe injection were collected from islets showing a robust MIP-GFP signal and apparently intact vasculature, immediately following i.v. tail vein injection of $E4_{\times 12}$-VT750 (0.2 nmol/g in 200 μL of a 10-μM solution, PBS). This dose was determined by fluorescence dose–response experiments for the fluorochrome chosen. Regions of interest (ROIs) were drawn within and outside the islets, and temporal changes were plotted using Prism 5.0a (GraphPad Software). Ex vivo ROIs were determined using pancreata that were excised 1 h after i.v. injection of the $E4_{\times 12}$-VT750 probe into MIP-GFP mice.

Immunohistochemistry and β-Cell Mass Estimation. The pancreata were embedded in OCT compound (Sakura Finetek) and flash-frozen in an isopentane bath on dry ice. The frozen tissues were sectioned (5-μm thickness), mounted on microscope slides, and stored at −80 °C. For insulin immunohistochemistry, the tissue sections were preincubated with 0.3% H_2O_2 to suppress endogenous peroxidase activity and then blocked with 5% (vol/vol) normal goat serum in PBS. Following the addition of a rabbit polyclonal insulin antibody (insulin H-86; Santa Cruz Biotechnology), a biotinylated anti-rabbit secondary antibody (Vector Laboratories, Inc.) was applied. The Vectastain ABC kit (Vector Laboratories, Inc.) and a 3-amino-9-ethylcarbazole substrate (Dako) were then used for color development. All the sections were counterstained with Harris hematoxylin solution. For overall morphology, H&E staining was also performed, and all images were captured using a NanoZoomer 2.0RS (Hamamatsu). β-cell mass was determined by thresholding and quantitating insulin-positive areas in nonadjacent sections at 50-μm intervals throughout pancreata according to published protocols (39). All images were digitized using a NanoZoomer 2.0RS. Color deconvolution was based on orthonormal transformation of the original RGB image. For each cohort, we analyzed a minimum of 15 individual whole-pancreatic histological slides (3 sections for each sample) containing ~40,000 × 40,000 pixels per image. Image processing was done using Matlab software (MathWorks).

Fluorescence Microscopy of Histological Slides. Fluorescence microscopy was performed at different wavelengths on the same sections of pancreata. GFP fluorescence was observed using a Chroma HQ FITC filter cube (HQ480/40× EX, dichroic Q505LP BS, and emission filter HQ535/50m EM; Chroma Technology Corp.), whereas, exendin-4 VT750 fluorescence was observed using a Chroma Cy7 filter cube (HQ775/50× EX, dichroic Q810LP BS, and emission filter HQ845/55m EM; Chroma Technology Corp.). All images were captured and processed using an epifluorescence microscope, Nikon Eclipse 80i (Nikon Instruments, Inc.), with a Cascade Model 512B camera (Roper Scientific).

STZ Treatment. Three cohorts of B6 mice at 14–18 wk of age received i.p. injections of STZ (Sigma–Aldrich) dissolved in 0.1 M sodium citrate (pH 4.5); mice received either a single injection of 75 mg/kg or 150 mg/kg of body weight, respectively, or 100 mg/kg of STZ daily for 5 d. Mice were given access to 10% (wt/vol) glucose-enriched water overnight to avoid hypoglycemia postinjection. Five days following STZ treatment, fluorescence- and histology-based whole-pancreas islet quantification was performed. Blood glucose levels from the tail vein were measured using the Contour Blood Glucose Monitoring System (Bayer HealthCare LLC).

Fluorescence-Based Whole-Pancreas Islet Quantification. After i.v. injection of $E4_{\times 12}$-VT750 (200 μL, 10 μM) and a 40-min time interval, untreated and STZ-treated mice were injected with heparin (~3 units of heparin, 300 μL of a 10-USP/mL solution) 10 min before euthanasia by CO_2 asphyxiation. B6 mice used for blocking experiments were injected with exendin-4 (250 μL, 60 μM, 20-min time interval) before i.v. injection with $E4_{\times 12}$-VT750 (200 μL, 10 μM, 40-min time interval) and then heparin (~3 units of heparin, 300 μL of a 10-USP units/mL solution) 10 min before euthanasia by CO_2 asphyxiation. The mice were then immediately perfused with 30 mL of PBS and heparin via the left ventricle. Likewise, 5 mL of PBS-heparin was perfused through the splenic artery to flush the pancreas completely. The organ was then excised,

weighed, and placed between two coverglass slides using a 1-mm rubber gasket to maintain a constant thickness. Fluorescence reflectance imaging of the entire pancreas was performed using an OV110 epifluorescence imager (Olympus) at low magnification (0.14×), equipped with standard filters for the 750-nm channel and a 2-s exposure. An ROI was drawn around the edges of the pancreas, and the average fluorescence signal was calculated using ImageJ (National Institutes of Health). For each cohort of mice, the autofluorescence signal in the pancreas was subtracted from mice receiving injections of only $E4_{\times 12}$-VT750 as well as from the respective mice injected with both $E4_{\times 12}$-VT750 and exendin-4; specific uptake was then determined by subtracting one from the other.

Laparoscopic Islet Imaging. Mouse pancreata were also imaged with a fiberoptic catheter-based imaging system in live mice using a laparoscopic approach; similar systems are used for microendoscopic purposes, such as imaging through the pancreatic duct in humans. The imaging system designed in-house includes a 1.6-mm outer diameter fiberoptic catheter and a 0.9-mm working channel coupled to an optical collection setup containing two high-resolution cameras (Pixelfly; PCO). Using this system, light collected from the fiberoptic catheter is divided into discrete white light and NIR beams by a 45° dichroic mirror. These beams are then focused onto the cameras, which enable simultaneous NIR (excitation/emission = 747/780–820 nm) and white light imaging. To perform islet imaging, animals were anesthetized with 2% isoflurane (vol/vol) in 2 L/min O_2 and fixed in a supine position with tape. The pancreas and surrounding organs were then surveyed using the fiberoptic catheter, in a similar manner to laparoscopic clinical procedures. Finally, the scanned area was also imaged using a confocal laser microscope (IV100) (37), operating at two different optical channels (488-nm excitation for MIP-GFP and 748-nm excitation for $E4_{\times 12}$-VT750). This was used to confirm that the observed fluorescent areas did indeed colocalize with MIP-GFP–expressing cells.

ACKNOWLEDGMENTS. We thank Yoshiko Iwamoto for histology and Rostic Gorbatrov for surgery. This work was supported, in part, by the following grants: National Institutes of Health (NIH) Grants P01 AI54904 (to D.M., C.B., and R.W.), U24 CA092782 (to R.W.), R01 67536 (to R.N.K.), and R01 EB006432 (to C.V.). C.W.L. was supported by Grant 1-K99-DK-090210-01 and NIH Training Grant 1RL9-EB-008539-01. R.U. is a Howard Hughes Medical Institute Medical Research Fellow. J.G. is supported in part by a KL2 Medical Research Investigator Training (MeRIT) award from Harvard Catalyst, the Harvard Clinical and Translational Science Center (NIH Award KL2 RR 025757), and the Harvard, Beth Israel Deaconess Medical Center Clinical Investigator Training Program. T.R. was supported by German Academy of Sciences Leopoldina Grant LPDS 2009-24.

1. Nakamoto Y, et al. (2000) Evaluation of pancreatic islet cell tumors by fluorine-18 fluorodeoxyglucose positron emission tomography: Comparison with other modalities. *Clin Nucl Med* 25:115–119.
2. Sweet IR, et al. (2004) Systematic screening of potential beta-cell imaging agents. *Biochem Biophys Res Commun* 314:976–983.
3. Moore A, Bonner-Weir S, Weissleder R (2001) Noninvasive in vivo measurement of beta-cell mass in mouse model of diabetes. *Diabetes* 50:2231–2236.
4. Schneider S, et al. (2005) In vitro and in vivo evaluation of novel glibenclamide derivatives as imaging agents for the non-invasive assessment of the pancreatic islet cell mass in animals and humans. *Exp Clin Endocrinol Diabetes* 113:388–395.
5. Harris PE, et al. (2008) VMAT2 gene expression and function as it applies to imaging beta-cell mass. *J Mol Med* 86:5–16.
6. Souza F, et al. (2006) Longitudinal noninvasive PET-based beta cell mass estimates in a spontaneous diabetes rat model. *J Clin Invest* 116:1506–1513.
7. Yong J, et al. (2011) Multimodality imaging of β-cells in mouse models of type 1 and 2 diabetes. *Diabetes* 60:1383–1392.
8. McGirr R, et al. (2010) Towards PET imaging of intact pancreatic beta cell mass: A transgenic study. *Mol Imaging Biol*, 10.1007/s11307-010-0435-5.
9. Toso C, et al. (2005) Positron-emission tomography imaging of early events after transplantation of islets of Langerhans. *Transplantation* 79:353–355.
10. Veluthakal R, Harris P (2010) In vivo beta-cell imaging with VMAT 2 ligands—Current state-of-the-art and future perspective. *Curr Pharm Des* 16:1568–1581.
11. Malaisse WJ, Louchami K, Sener A (2009) Noninvasive imaging of pancreatic beta cells. *Nat Rev Endocrinol* 5:394–400.
12. Souza F, et al. (2006) Current progress in non-invasive imaging of beta cell mass of the endocrine pancreas. *Curr Med Chem* 13:2761–2773.
13. Ahlgren U, Gotthardt M (2010) Approaches for imaging islets: Recent advances and future prospects. *Adv Exp Med Biol* 654:39–57.
14. Martinic MM, von Herrath MG (2008) Real-time imaging of the pancreas during development of diabetes. *Immunol Rev* 221:200–213.
15. Christoffersson G, et al. (2010) Clinical and experimental pancreatic islet transplantation to striated muscle: Establishment of a vascular system similar to that in native islets. *Diabetes* 59:2569–2578.
16. Ntziachristos V, Ripoll J, Wang LV, Weissleder R (2005) Looking and listening to light: The evolution of whole-body photonic imaging. *Nat Biotechnol* 23:313–320.
17. Alanentalo T, et al. (2010) Quantification and three-dimensional imaging of the insulitis-induced destruction of beta-cells in murine type 1 diabetes. *Diabetes* 59: 1756–1764.
18. Alanentalo T, et al. (2007) Tomographic molecular imaging and 3D quantification within adult mouse organs. *Nat Methods* 4:31–33.
19. Lin KY, Maricevich M, Bardeesy N, Weissleder R, Mahmood U (2008) In vivo quantitative microvasculature phenotype imaging of healthy and malignant tissues using a fiber-optic confocal laser microprobe. *Transl Oncol* 1:84–94.
20. Corbin KL, Hall TE, Haile R, Nunemaker CS (2011) A novel fluorescence imaging approach for comparative measurements of pancreatic islet function in vitro. *Islets* 3: 14–20.
21. Takahashi N, et al. (2002) Two-photon excitation imaging of pancreatic islets with various fluorescent probes. *Diabetes* 51(Suppl 1):S25–S28.
22. Ahrén B (2009) Islet G protein-coupled receptors as potential targets for treatment of type 2 diabetes. *Nat Rev Drug Discov* 8:369–385.
23. Ho NH, Weissleder R, Tung CH (2006) Development of a dual fluorogenic and chromogenic dipeptidyl peptidase IV substrate. *Bioorg Med Chem Lett* 16:2599–2602.
24. Reiner T, et al. (2010) Near-infrared fluorescent probe for imaging of pancreatic beta cells. *Bioconjug Chem* 21:1362–1368.
25. Widmann C, Dolci W, Thorens B (1995) Agonist-induced internalization and recycling of the glucagon-like peptide-1 receptor in transfected fibroblasts and in insulinomas. *Biochem J* 310:203–214.
26. Rostovtsev VV, Green LG, Fokin VV, Sharpless KB (2002) A stepwise huisgen cycloaddition process: Copper(I)-catalyzed regioselective "ligation" of azides and terminal alkynes. *Angew Chem Int Ed Engl* 41:2596–2599.
27. Like AA, Rossini AA (1976) Streptozotocin-induced pancreatic insulitis: New model of diabetes mellitus. *Science* 193:415–417.
28. Kelly KA, et al. (2005) Detection of vascular adhesion molecule-1 expression using a novel multimodal nanoparticle. *Circ Res* 96:327–336.
29. Weissleder R, et al. (2000) In vivo magnetic resonance imaging of transgene expression. *Nat Med* 6:351–355.
30. Buchner AM, et al. (2011) The learning curve of in vivo probe-based confocal laser endomicroscopy for prediction of colorectal neoplasia. *Gastrointest Endosc* 73:556–560.
31. Gheonea DI, et al. (2010) Confocal laser endomicroscopy of the colon. *J Gastrointestin Liver Dis* 19:207–211.
32. Thurber GM, Figueiredo JL, Weissleder R (2010) Detection limits of intraoperative near infrared imaging for tumor resection. *J Surg Oncol* 102:758–764.
33. Figueiredo JL, Nahrendorf M, Vinegoni C, Weissleder R (2011) Intraoperative near-infrared fluorescent cholangiography (NIRFC) in mouse models of bile duct injury: Reply. *World J Surg* 35:694–695.
34. Miyazaki J, et al. (1990) Establishment of a pancreatic beta cell line that retains glucose-inducible insulin secretion: Special reference to expression of glucose transporter isoforms. *Endocrinology* 127:126–132.
35. Gromada J, Rorsman P, Dissing S, Wulff BS (1995) Stimulation of cloned human glucagon-like peptide 1 receptor expressed in HEK 293 cells induces cAMP-dependent activation of calcium-induced calcium release. *FEBS Lett* 373:182–186.
36. Liew CW, et al. (2010) The pseudokinase tribbles homolog 3 interacts with ATF4 to negatively regulate insulin exocytosis in human and mouse beta cells. *J Clin Invest* 120:2876–2888.
37. Alencar H, Mahmood U, Kawano Y, Hirata T, Weissleder R (2005) Novel multiwavelength microscopic scanner for mouse imaging. *Neoplasia* 7:977–983.
38. Hara M, et al. (2003) Transgenic mice with green fluorescent protein-labeled pancreatic beta-cells. *Am J Physiol Endocrinol Metab* 284:E177–E183.
39. Montanya E, Téllez N (2009) Pancreatic remodeling: Beta-cell apoptosis, proliferation and neogenesis, and the measurement of beta-cell mass and of individual beta-cell size. *Methods Mol Biol* 560:137–158.